이학석사 학위논문

파랑후측에서 나타난 동해 파랑 기후의 선형 추세

Linear trend of wave climate in the East Sea estimated from wave hindcast

지도교수 장찬주

2020년 2월

한국해양대학교 해양과학기술전문대학원

해양과학기술융합학과

김 기 호

본 논문을 김기호의 이학석사 학위논문으로 인준함.

위원장 도 기 덕 (인)

위 원 장 찬 주 (인)

위 원 유 제 선 (인)

2019년 12월 16일

한국해양대학교 해양과학기술전문대학원

Index

List of Tables

List of Figures

파랑후측에서 추정한 동해 파랑기후의 선형추세

김 기 호

한국해양대학교 해양과학기술전문대학원
해양과학기술융합학과

초록

파랑기후의 변화는 연안 침식과 해안선 변화 등 연안 환경에 많은 영향을 준다. 최근 우리나라 동해안에 고파랑에 의한 피해가 증가함에 따라 고파랑 연구가 활발하게 진행되고 있다. 하지만 파고와 함께 연안 환경에 영향을 주는 파의 주기와 방향에 대한 연구는 상대적으로 부족하다. 따라서 본 연구에서는 SWAN 파랑모형과 ERA-Interim 재분석 바람자료를 이용하여 40년(1979~2018) 기간의 파랑을 재현하였으며, 이를 통해 동해에서 풍속, SWH, PWP, PWD을 분석하였다. 유의파고와 첨두주기의 40년 장기평균은 북서쪽에서 남동쪽 해역으로 갈수록 증가하는 공간분포를 보이며, 이러한 공간분포는 겨울철 장기 평균과 상당히 유사하다. 이는 겨울 공간분포가 장기 공간분포에 크게 영향을 준다는 것을 의미한다. 첨두파향의 장기 평균은 강한 북서풍의 영향으로 동해 남동쪽 해역에서 북서계열의 파가 우세하며, 서쪽으로 갈수록 반시계방향으로 변화하여 우리나라 연안에서는 남동~북동계열

파가 나타났다. 동해는 계절풍의 영향으로 계절별 풍향 변화가 크기 때문에 풍향에 크게 영향을 받는 파향 역시 뚜렷한 계절변동을 보인다. 하지만 동해 남서쪽 해역인 포항 연안에서는 북동~남동계열의 파가, 동해 남동쪽 해역인 일본 연안에서는 북서계열의 파가 연중 지속된다. 99 백분위수 유의파고와 첨두주기는 동일하게 동해 대부분의 영역에서 증가하는 추세를 보이며, 특히 동해 남동쪽 해역에서 가장 크게 증가한다. 첨두주기와 99 백분위수 유의파고 월별 평균은 비슷한 공간분포를 보이지만, 선형추세는 다르게 나타난다. 풍속 추세에 영향을 크게 받아 99 백분위수 유의파고 추세는 시, 공간 변화가 크게 나타나는 반면, 첨두주기는 8~10월 동해 북쪽 해역에서 감소를 제외하고 대부분 증가하는 추세를 보인다.

.

KEY WORDS: 파랑 기후; 선형추세; 동해; 파랑 후측

Linear trend of wave climate in the East Sea estimated from wave hindcast

Kim, Ki Ho

Department of Convergence Study on the Ocean Science and Technology
School of Ocean Science and Technology
Korea Maritime and Ocean University

Abstract

Changes in ocean wave climate influences the costal environments such as coastal erosion and coastline change. Many studies are being conducted about the high wave height, since high wave impacts on the east coast of Korea, recently. However, relatively few researches are investigated by the wave period and direction which affect the coastal environment with the wave height. In this study, we investigate the wind speed, significant wave height (SWH), peak wave period (PWP), and peak wave direction (PWD) in the East Sea, using a 40 years (1979~2018) wave hindcast experiment conducted by using the SWAN wave model forced with the ECMWF reanalysis wind data. The long-term mean of the PWP and monthly-mean and 99th percentile SWH showed high value in the southeastern area, while low value in the northwestern area. This spatial distribution is considerably similar to that of December, which means that the spatial distribution of December significantly influences long-term mean. The prevailing of the

long-term mean of PWD is northwesterly in the southeastern area and translate an anti-clockwise toward the east coast of Korea. In association with the apparent seasonally-varying wind data by the Asian monsoon, the long-term mean of wave properties shows obviously differ in seasons. Nevertheless, throughout the year, there are predominant from northeasterly to southeasterly waves in the southwestern area, and northwesterly waves in the southeastern area. The PWP and monthly-mean and 99th percentile SWH appear an increasing trend in most of the area, especially, in the southeastern basin show a noticeable increasing trend. The spatial distribution of the monthly mean of the 99th percentile SWH and PWP show a similar pattern, while that of the linear trends appear differently. The trend of the 99th percentile SWH considerably alter in accordance with locations and seasons, while, the PWP tends to increase in most of the East Sea except the northern area from August to October.
KEY WORDS: wave climate; linear trend; East Sea; wave hindcast

1. Introduction

Changes in ocean wave climate due to climate change affect the coastal environments such as coastal erosion and coastline change. Recently, because extreme wave heights greatly impacted the coastal environment, many researchers have studied the long-term trend of significant wave height (SWH) to prevent and mitigate damage (e.g. Allan et al., 2000; Cox and Swail, 2001; Wang and Swail, 2002; Yamaguchi and Hatada, 2003; Sasaki et al., 2005; Ruggiero et al., 2010b; Young et al., 2011; Zheng et al., 2013; Zheng and Li, 2015; Castelle et al., 2018). In addition, studies of the wave period and wave direction which influence the coastal environment with wave height are increasing (e.g. Dupuis et al., 2006; Weisse and Guther, 2007; Dodet et al., 2010; Harley et al., 2010; Raamet et al., 2010; Charles et al., 2012; Duan et al., 2014; Zhang et al., 2018).

Most of the studies of SWH in the Northeast Pacific have used observation data (Allan et al., 2000; Ruggiero et al., 2010b). Linear trend of SWH in the East Sea showed different results by study period and used model. Among the studies of SWH in the Northwest Pacific including in the East Sea, Sasaki et al. (2005) performed wave hindcasting by using the WWⅢ wave model forced with National Center for Environmental Prediction (NCEP) and National Center for Atmospheric Research (NCAR) reanalysis wind data during 25 years (1980~2004) and found that the SWH had an increasing trend in the southern East Sea, while a decreasing trend in the northern East Sea. Yamaguchi and Hatada (2013) conducted wave hindcasting by using shallow water wave model forced with NCEP/NCAR reanalysis wind data during 41 years (1958~1998) and

observed the SWH showed a decreasing trend in the East Sea.

Recently, as increasing the hazard by the extreme wave heights in the Korea east coast (Go et al., 2006; Jeong and Oh, 2009; Choi and Lee, 2010), many researchers were studying of the long-term trend SWH in the East Sea (Jeong et al., 2016; Kang et al., 2016; Woo and Park, 2017). Although the East Sea is a semi-closed marginal sea, East Sea was frequently referred as a "miniature ocean" because it exhibited oceanic phenomena and processes (Gamo and Horibe, 1983). Due to the steepness water depth change high SWH frequently influenced the Korea east coast, it seemed to need analysis long-term trend of SWH in the East Sea. Jeong et al. (2016) investigated an annual variability of SWH at the observation buoy near the Korea coast, a 36 years (1979~2014) wave hindcast data obtained from SWAN (Simulating WAves Nearshore) wave model force with ECMWF (European Centre for Medium-range Weather Forecasts) reanalysis wind data. Trend of SWH showed an increasing along the coast of Korea and southern basin and recent period (1994~2014) more increase than northern basin and whole period (1979~2014). Kang et al. (2016) analyzed appearance ratio trend for waves of more than 2 m in height at coastal waters near Korea, based on wave hindcasting using SWAN wave model forced with ECMWF reanalysis wind data during 14 years (2001~2014). An increased appearance ratio trend entire of the East Sea and the trend of the ratio in the southern area is bigger than in the northern area. Woo and Park (2017) estimated the long-term trend of monthly-mean and extreme SWH and its monthly spatial distribution using data of IFREMER (Institut Francais de Recherche pour l' Exploitation de la Mer) nine satellite altimeters. However, above two research's reanalysis wind data was low-resolution (< 1/2°) so that there was a limit to simulate detail regional distribution and because of the short study period (25 years), to analyze the long-term trend was limited, and investigated the spatial distribution of SWH.

Such research have been done about long-term trend of SWH, while wave period and direction have been less studied (Kim et al., 2011a; Jeong et al., 2015). Kim et al. (2011a) conducted wave hindcasting by using SWAN wave model forced with ECMWF wind data during 25 years (1979~2003) and analyzed peak wave direction (PWD) at the four-station near Korea. Wave direction in the East Sea significantly varied depending on regions and seasons, especially northeastern waves had frequent regardless of the season, at the eastern point (near Pohang). Based on 12 years (2003~2014) time-series of buoy data in the Sokcho, Jeong et al. (2015) analyzed monthly mean of SWH and peak wave period (PWP). Two studies respectively have a limit: using low-resolution reanalysis wind data and using buoy data that do not have data before 2002 and have many missing data. Although previous studies performed wave properties (SWH, PWP, PWD) most of the research studied only at the several buoy data, and there were few studies investigated the relationship between wind speed and SWH, and spatial distribution of the wave properties. In this study, to investigate the spatial distribution of the wind speed and wave properties in the East Sea, using a 40 years (1979~2018) wave hindcast experiment obtained from a high-resolution wave model (SWAN) simulation forced with the ECMWF reanalysis wind field.

2. Data and methods

2.1 Wave model

Many surface waves (e.g. capillary wave, wind wave, swell, wind surge, tsunami, tide) generate on the sea surface due to various external forces (e.g. surface tension, wind, storms, earthquake, changes in the attraction on the sun and moon). If all of these waves are included, wave frequency distribution is a wide range from 10^{-6} Hz to 10^{2} Hz. Generally, waves third-generation wave models (WAM, WW Ⅲ, SWAN) were used to analyze surface. The WAM and WW Ⅲ wave models, developed for deep water, do not consider shallow water processes (Chun et al., 2011; Kim et al., 2011b; Suh et al., 2011) so they are difficult to apply in shallow water. On the other hand, SWAM model's numerical propagation scheme is implicit which means SWAN calculates more effective in shallow water. In this study, we used the SWAN cycle Ⅲ version 40.72 third generation spectral wave model developed at the Delft University of Technology (Booji et al., 1999; Ris et el., 1999).

2.1.1 Governing equation

The SWAN wave model is based on the wave action balance equation (Equation 1).

$$\frac{\partial N}{\partial t}+\frac{\partial c_x N}{\partial x}+\frac{\partial c_y N}{\partial y}+\frac{\partial c_\sigma N}{\partial \sigma}+\frac{\partial c_\theta N}{\partial \theta}=\frac{S}{\sigma} \quad (1)$$

where σ is the frequency, c_x, c_y, c_σ, c_θ are the propagation velocity in the

x, y, σ, θ components respectively. The action density spectrum ($N(\sigma,\theta)$) and the energy density spectrum ($E(\sigma,\theta)$) have a relationship of Equation (2).

$$N(\sigma,\theta) = E(\sigma,\theta)/\sigma \tag{2}$$

In Equation (1), the right-hand side S the source term which represent effects of generation, dissipation and non-linear wave-wave interactions (Equation 3).

$$S = S_{in} + S_{ds} + S_{nl} \tag{3}$$

S_{in} is generation due to wind input, S_{ds} is dissipations due to bottom friction, wave breaking, S_{nl} is a nonlinear transfer of wave energy through quadruplet wave-wave interactions. In SWAN wave model, wave growth by wind is described by Equation (4),

$$S_{in}(\sigma,\theta) = A + B \cdot \quad E(\sigma,\theta) \tag{4}$$

A describes linear component of wave growth which depends on wave frequency and direction, and $B \cdot E$ is the exponential component which depends on wind speed and direction.

For the linear component of wave growth term A is due to Cavaleri and Malanotte-Rizzoli (1981) (Equation (5), (6)),

$$A = \frac{1.5 \times 10^{-3}}{2\pi g^2}[U_* \max(0, \cos(\theta - \theta_W))]^4 H \tag{5}$$

$$H = \exp(\frac{\sigma}{\sigma^*_{PM}})^{-4}, \sigma^*_{PM} = \frac{0.13g}{28U_*} \tag{6}$$

in which θ_W is the wind direction, σ^*_{PM} is the peak frequency of the fully developed sea in accordance with friction velocity from Pierson and Moskowitz (1964). Equation (5) is with a filter to eliminate wave growth at frequencies lower than the Pierson-Moskowtiz frequency (Tolman, 1992).

There are two equations for the exponential component of wave growth by the wind: the first is Janssen (1989, 1991), the second is Komen et al. (1984). In this study use Equation (7) due to Komen et al. (1984).

$$B = \max[0, 0.25\frac{\rho_a}{\rho_W}(28\frac{U_*}{C_{ph}}cos(\theta-\theta_W)-1]\sigma \quad (7)$$

In which U_* is the friction velocity, C_{ph} is the phase speed and, ρ_a, ρ_W are the density of air and water, respectively.

2.1.2 Model domain

The model domain was implemented on a 1/25° resolution grid (375×439) on a spherical coordinate covering the East Sea (34.89~52.41° N, 127.34~142.30° E). The bathymetry originated from the GEBCO 08 (Becker et al., 2009) and wind fields obtained from ERA-Interim six-hourly wind data. Directional resolution is 10° , and frequency space is 0.05~1 Hz, which was discretized in 24 increments logarithmically. A 40-year simulation was performed from 1979 to 2018 and the wave properties such as SWH, PWP, and PWD were archived every 6 hours with a time step of 30 minutes. Generally, the spin-up time of the wave model is approximately 1~2 days (Park et al., 2013). However, there is a possibility of a long spin-up time when wind speed is strong such as December the initial condition for our research. Therefore in this study, the wave model simulated 9-day for the spin-up. Although SWH is considerably affected by swell at a global scale, it is negligible effects in the East Sea which is the semi-closed marginal sea. Therefore, swell propagated northwards on the southern boundary from the northwestern Pacific ocean was ignored.

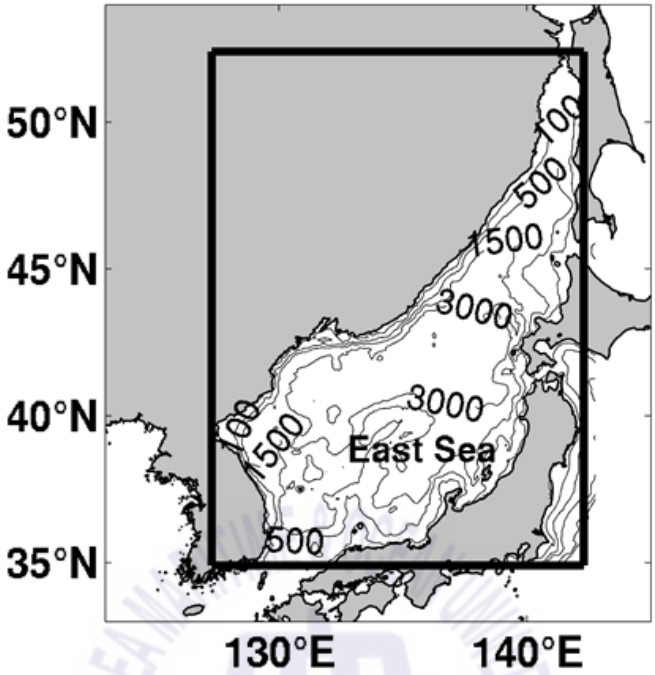

Fig. 1 Model domain with bottom topography on a 1/25° × 1/25° grid. The black box represents the regions for detailed analysis.

Table 1 Introduction of wave numerical modeling

Model	SWAN
Study period	40-year (1979~2018)
Model domain	127.58~141.82° E (375 grids) 34.89~52.41° N (439 grids)
Spatial resolution	0.04°
Bathymetry	GEBCO 08
Wind data	ERA-Interim (0.125° , 6h)
Frequency space	24 bins from 0.05 to 1 Hz (1~20 s)
Directional space	36 bins of 10°

2.2 Methodology

To analyze the linear trend of mean and extreme wave climate, PWP, PWD, monthly-mean and 99^{th} percentile wind speed and SWH were used. Monthly-mean value is the monthly mean of the model result archived 6 hours, the 99^{th} percentile value is 99^{th} percentile among the month. The 99^{th} percentile value is calculated by linear interpolation, not the actual value, represents an extreme value equal to the upper 1% of SWH. PWP and PWD are the wave period and direction with most energetic waves in the total wave spectrum.

We separated the East Sea into three areas: A, B, and C to investigate the spatiotemporal change of the wind speed and SWH and observed relationship between wind speed and SWH. A area is 37.01~38.01° N, 129.54~130.54° E where the east coast of Korea, recently increases coastal erosion, B area is 39.49~40.49° N, 137.42~138.42° E where the southeastern basin, is occurred high SWH by the northwesterly wind in winter. C area is 44.01~45.01° N, 139.70~140.70° E where the maximum annual wind speed is located.

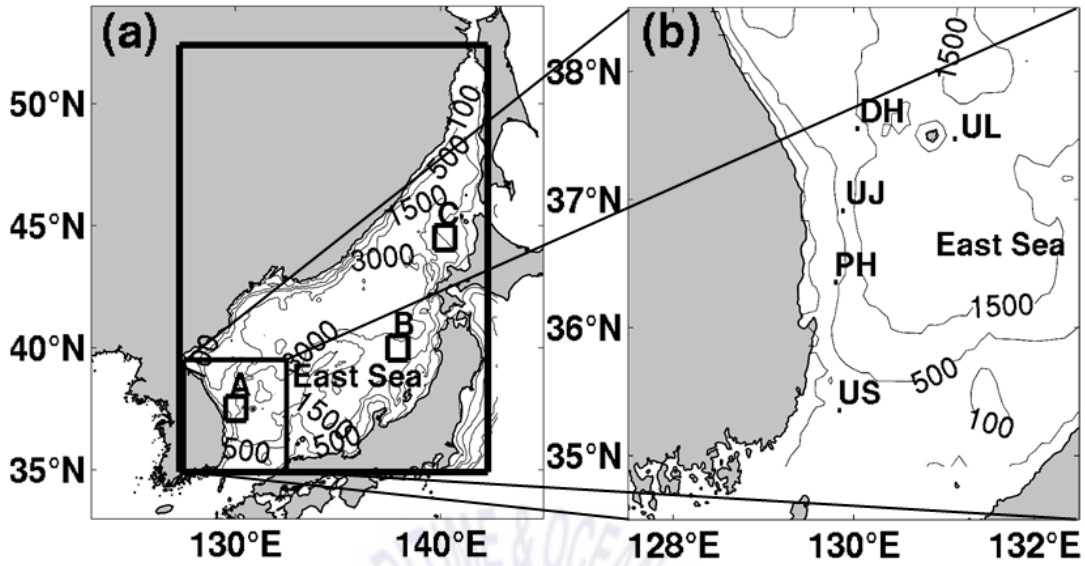

Fig. 2 (a) Model domain with bottom topography on a 1/25° × 1/25° grid. The black boxes represent the regions for detailed analysis: A: East sea coast, B: high significant wave height area, C: high wind speed area. (b) Locations of the wave measurement stations (UL: Ulleungdo, DH: Donghae, UJ: Uljin, PH: Pohang, US: Ulsan) in the East Sea operated by KMA (Korea Meteorological Administration).

As wind speed is strong, wave height is high, especially for extreme conditions wind speed and wave height have a strong correlation (Young et al., 2011). Generally in summer, as wind speed is weak, wave height is lower than winter. However, high SWH is occurred by the strong wind speed when typhoon pass. To investigate the number of typhoons affect summer high SWH, we research the number of typhoons that pass 34~42° N, 127~134° E during 1979~2018, using Japan Meteorological Agency (JMA) typhoon track data. During 40 years, 2.65 typhoons passed per year, most frequently in August (37), followed by September (32) and July (25) (fig 3). The number of typhoons passed July to September was about 86 %, sometimes typhoons

passed in June and October. According to previous research, the number of typhoons decreased and intensity increased in the northwest Pacific (Emanuel, 2005; Webster et al., 2005; Wu et al., 2006; Mei et al., 2015). The number of typhoons affecting Korea showed a decreasing trend, but that of typhoons through the East Sea appeared an increasing trend (Seol, 2010). When intense typhoon occurs it causes intense wind speed and increases SWH affected by wind speed. When intense typhoons pass frequently, high SWH occur frequently, so August, when typhoons passed most frequently, was selected as the representative season of summer.

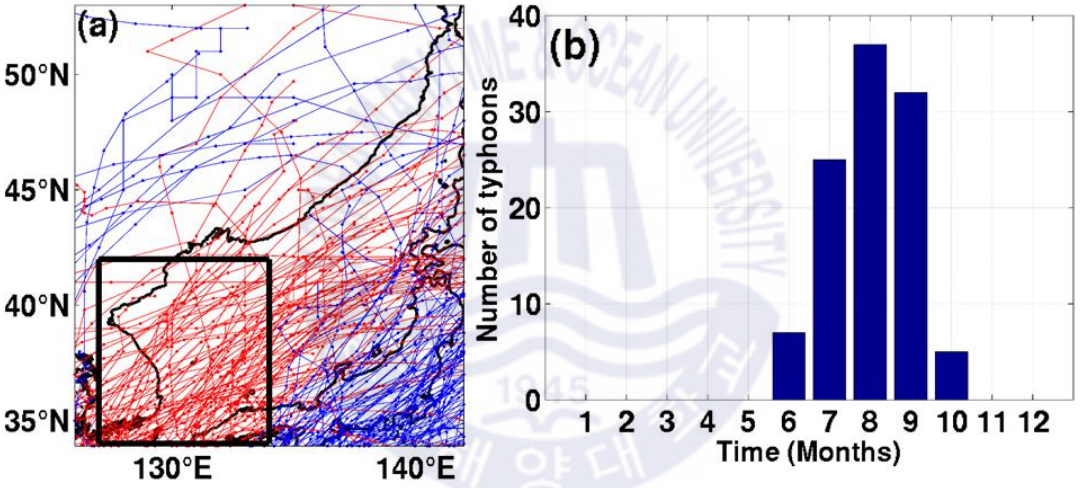

Fig. 3 (a) Typhoons where the center passed through 34~42° N, 127~134° E over the period from 1979 to 2018 (red line). (b) The number of monthly typhoons that have passed through the area.

As a result of analyzing the 99th percentile wind speed in winter (November to February) when strong northwesterly winds are dominant, the mean was the highest in December, followed January and November, and the increasing trend was the largest in December, followed November and January. When the 99th percentile wind speed is intense and large increasing, high SWH is

greatly high and increasing, so December was chose as the representative season of winter.

Table 2 Mean and trend of winter wind speed

Wind speed	Mean(m/s)		Trend(cm/s/yr)	
	Monthly mean	99^{th} percentile	Monthly mean	99^{th} percentile
Nov	7.25	14.94	0.16	2.77
Dec	7.39	15.42	1.87	4.06
Jan	7.99	15.29	0.11	2.10
Feb	7.37	14.90	0.43	1.67

In general, SWH and PWP are known to have a positive correlation, and several formulas have been suggested a relationship between SWH and PWP (Shore protection manual, 1977; Goda, 2003; Suh et al., 2010). Especially, due to when SWH is high, the correlation of SWH and PWP is higher, we analyzed the 99^{th} percentile SWH and PWP that are greater than the significant wave height and significant wave period. Wind speed and direction in the East Sea differ depending on seasons due to the monsoon. Therefore, we analyzed monthly the long-term mean and linear trend of the wind speed and wave climate (SWH, PWP, PWD) in the East Sea.

3. Results

3.1 Significant wave height and wind speed

3.1.1 Model validation

We validated the model result by the comparison with the buoy data at five locations (Ulleungdo, Donghae, Uljin, Pohang, Ulsan) (table 3) around the East Sea (fig 2b). The wave buoy was conducted by Korea Meteorological Agency (KMA). Due to different monitoring period at five buoys, we used 2016 data which have the least missing value during the common observation period. To detect outlier of observation data using Rosner test (Rosner, 1983), as a result, no outlier was found in the result ($p < 0.05$). Model results underestimated at all of five buoys. Previous research also performed wave hindcast experiment by using the SWAN wave model forced with ECMWF wind data in the East Sea, consequently, the model results underestimated (Jeong et al., 2016; Heo et al., 2017; Do and kim, 2018). As well as the East Sea other regions also showed that model results underestimated (Akpinar et al., 2012; Charles et al., 2012; Pallares et al., 2014; Kazeminezhad and Siadatmousavi, 2017). In other research, cause the model results underestimated, first is the weakness of accurately simulating the change of wind direction (Cardone et al., 1996; Cavaleri, 2009; Akpinar et al., 2012; Jeong et al., 2016; Kazeminezhad and Siadatmousavi, 2017; Caries et al., 2018) and underestimation extreme wind speed, due to the coarse spatiotemporal resolution of wind data, second is that model misses the peak wave height (Cardone et al., 1996; Cavaleri, 2009; Akpinar et al., 2012) because of the

model resolution. However, when compared with observation wind speed and ERA-Interim wind speed in 2016, ERA-Interim underestimated at Uljin, Pohang, and Ulsan buoy, while overestimated at Ulleungdo and Donghae buoy. For this reason, semi-closed marginal sea, wave model, wind data, etc. are considered complex result, further study is needed.

Table 3 Information of the wave monitoring stations

Symbol	Station	Latitude (° N)	Longitude (° E)	Monitoring Period
Ul	Ulleungdo	37.3443	131.1144	2011. 12. 28 ~ Present
DH	Donghae	37.5442	130.0000	2001. 04. 01 ~ Present
UJ	Uljin	36.9069	129.8744	2015. 12. 09 ~ Present
PH	Pohang	36.3500	129.7833	2008. 11. 15 ~ Present
US	Ulsan	35.3453	129.8414	2015. 12. 22 ~ Present

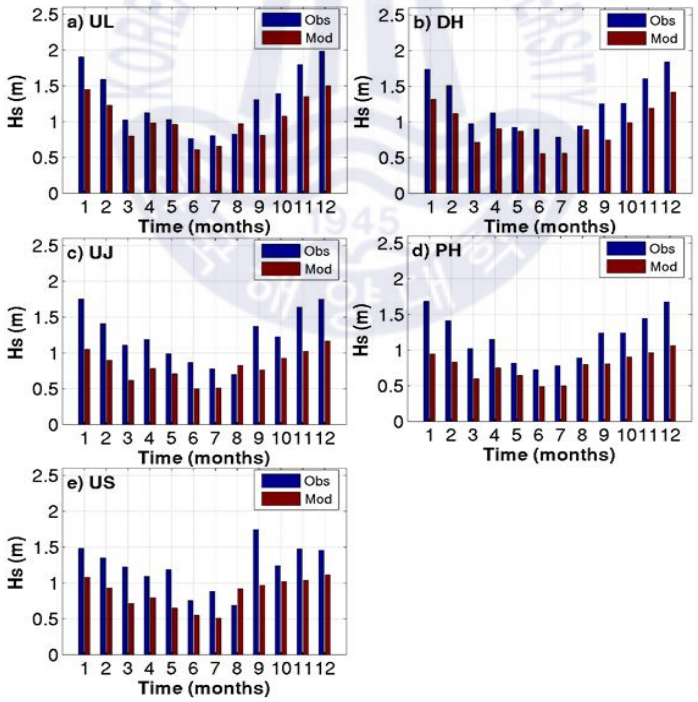

Fig. 4 Comparison of hindcast and observation of monthly mean significant wave height in 2016: (a) UL, (b) DH, (c) UJ, (d) PH, and (e) US.

3.1.2 Long-term mean of wind speed and SWH

In this study, we separated the East Sea into three areas: A, B, C to analyze wind speed and SWH each area and investigate the correlation of the spatial distribution of the wind speed and SWH. The monthly-mean SWH showed high value (> 1 m) in the southeastern area, while low value (< 1 m) in the northwestern area (fig 5b). The maximum value of wind speed (7.4 m/s) showed in C area (fig 5a), SWH (1.2 m) showed in B area, relatively southern region. The reason why different located of the maximum of the wind speed and SWH is due to the fetch length in which affects wave growth by the Siberian northwesterly monsoon in winter. According to previous research, when strong northwesterly wind blew (> 15 m/s) continuously more than one day, high SWH occurred in the southeastern area, which is known to fetch-limited wave growth (Ebuchi et al., 1992; Ebuchi, 1999). On the other hand, in the northwestern area showed relatively low SWH owing to limit fetch length by the Hamgyeong Mountains of Korea and Sikhote-Aline Mountains of Russia. When fetch length is long, high SWH appears, which this phenomenon is observed where strong winds blow continuously like in Australia, South America, and Africa (Young, 1994; Chen et al., 2002).

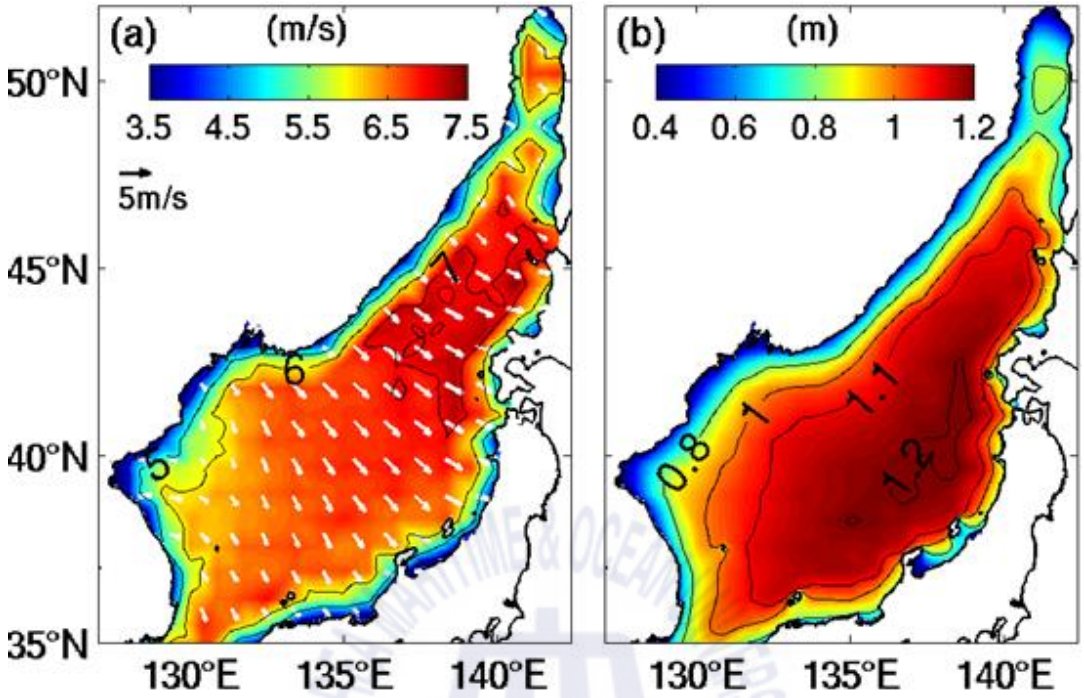

Fig. 5 Spatial distribution of 40-year (1979~2018) mean of (a) wind speed (m/s) and (b) significant wave height (m) in the East Sea. In (a), wind vectors are overlaid on wind speed.

Spatial distribution of 40-year mean of wind speed and SWH were similar to in December, when strong northwesterly winds are dominant. It means that the spatial distribution of the long-term mean of wind speed and SWH were influenced by December. In the entire East Sea, December mean of wind speed and SWH were 7.9 m/s, 1.4 m respectively, maximum were 9.5 m/s, 1.9 m respectively. The maximum values were respectively 1.2, 1.4 times larger than that of the mean values. Besides due to the mean of wind speed in December stronger than the long-term mean, the maximum SWH in December located in the southeast than the long-term mean. In December, due to the fetch length, it showed a different spatial distribution in the maximum value:

SWH located south of 40 ° N, wind speed located north of 40 ° N, while in August, SWH and wind speed showed a similar spatial distribution that decreased from the center to the northwest and southeast (fig 6a, b).

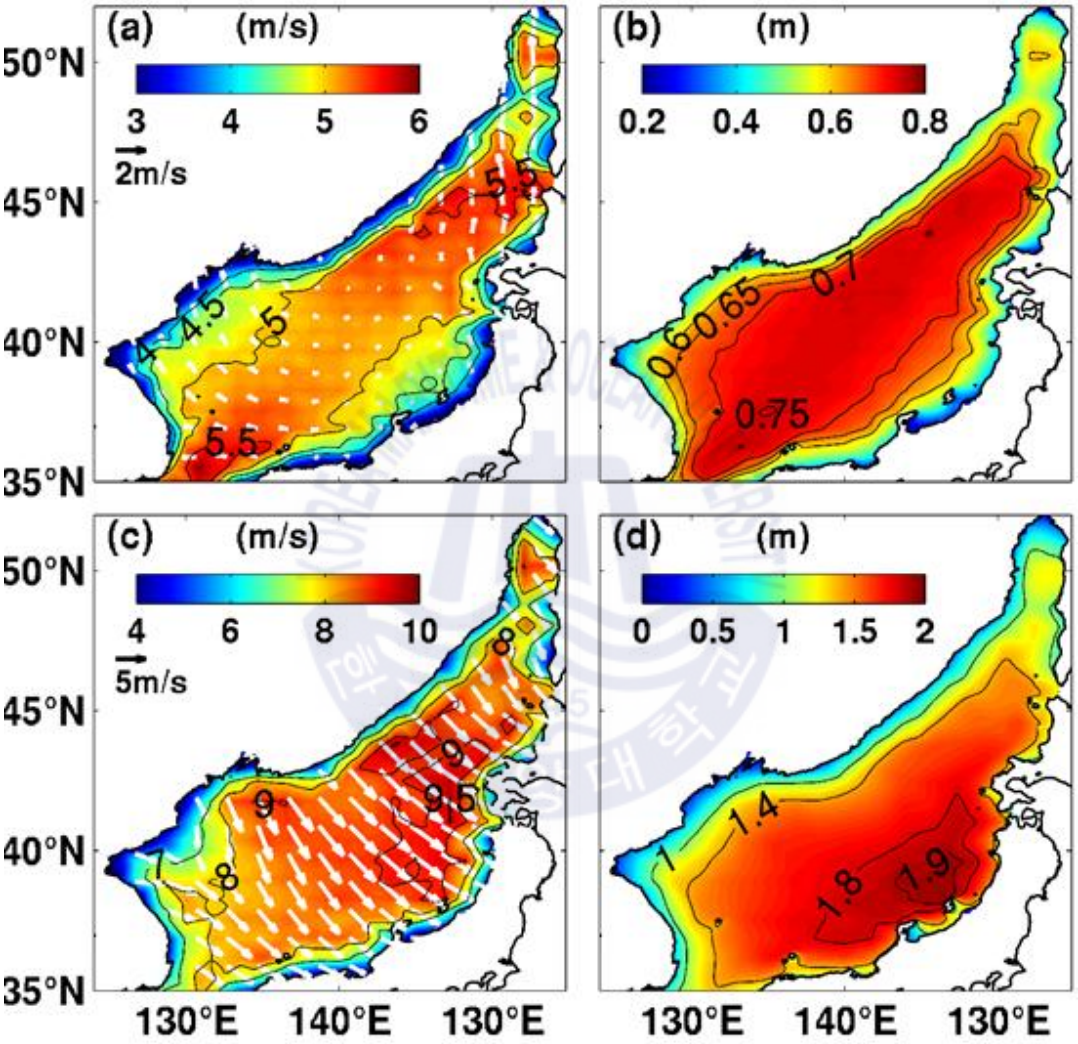

Fig. 6 Spatial distribution of monthly mean of wind speed (left panel) and significant wave height (right panel) in the East Sea averaged over the period from 1979 to 2018: August (upper) and December (lower). In (a) and (c), wind vectors are overlaid on wind speed.

As a result of comparing the mean of the monthly-mean and 99th percentile wind speed and SWH by area, the amplitude of winter was higher than summer, and wind speed and SWH had a positive correlation (fig 7). In A area, monthly-mean and 99th percentile SWH showed lower than the other regions, whereas, in August, 99th percentile SWH showed high value (2.9 m) similar to B area where high SWH appeared. The monthly-mean and 99th percentile of wind speed in the C area were 7.1 m/s, 14.7 m/s respectively, they were higher than 6.8 m/s, 14.6 m/s in the B area. However, the monthly-mean and 99th percentile of SWH in the C area were 1.1m, 3.5 m respectively, they were lower than 1.2 m, 3.8 m in the B area. The reason why the locations of the high value of the wind speed and SWH were different, which is caused by the difference in the fetch length as mentioned previously.

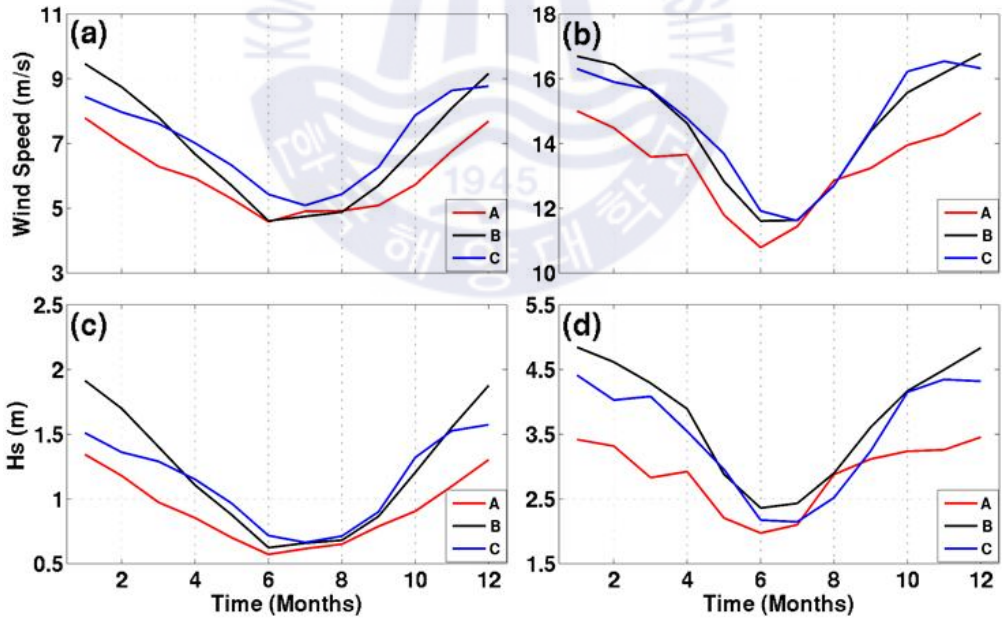

Fig. 7 Monthly variation of monthly mean (left panel) and 99th percentile (right panel) at three areas (A, B, & C) averaged over 40 years (1979~2018): wind speed (upper) and significant wave height (lower).

3.1.3 Long-term trend of wind speed and SWH

We analyzed the trends of the monthly spatial distribution to investigate long-term trend and correlation of the spatial distribution of the wind speed and SWH. In August, the monthly-mean SWH showed an increasing trend (1.0 cm/s/yr) in the southeastern area and from East Korea Bay to near Vladivostok, while showed a decreasing trend (1.0 cm/s/yr) in other regions. The amplitude of the trend of the 99th percentile wind speed was greater than the monthly-mean. Spatial distribution showed an increasing trend from the western basin to the Soya Straits along the coast of North Korea and Russia, except East Korea Bay and near Vladivostok, and showed a decreasing trend in the southeastern basin. It is considered that typhoons, most frequently passed in August, influenced the 99th percentile wind speed. In December, both the monthly-mean and 99th percentile wind speed showed an increasing trend in most of the East Sea. Especially, the maximum value of increasing trend located in the southeastern East Sea, which were 5.0 cm/s/yr, 11.0 cm/s/yr respectively (fig 8b, d). As the intensity of the Siberian High increased (Sun et al., 2016; Kim et al., 2018; Zhao et al., 2018) and the difference between the Siberian High and the East Sea pressure increased, the northwesterly winds became strong.

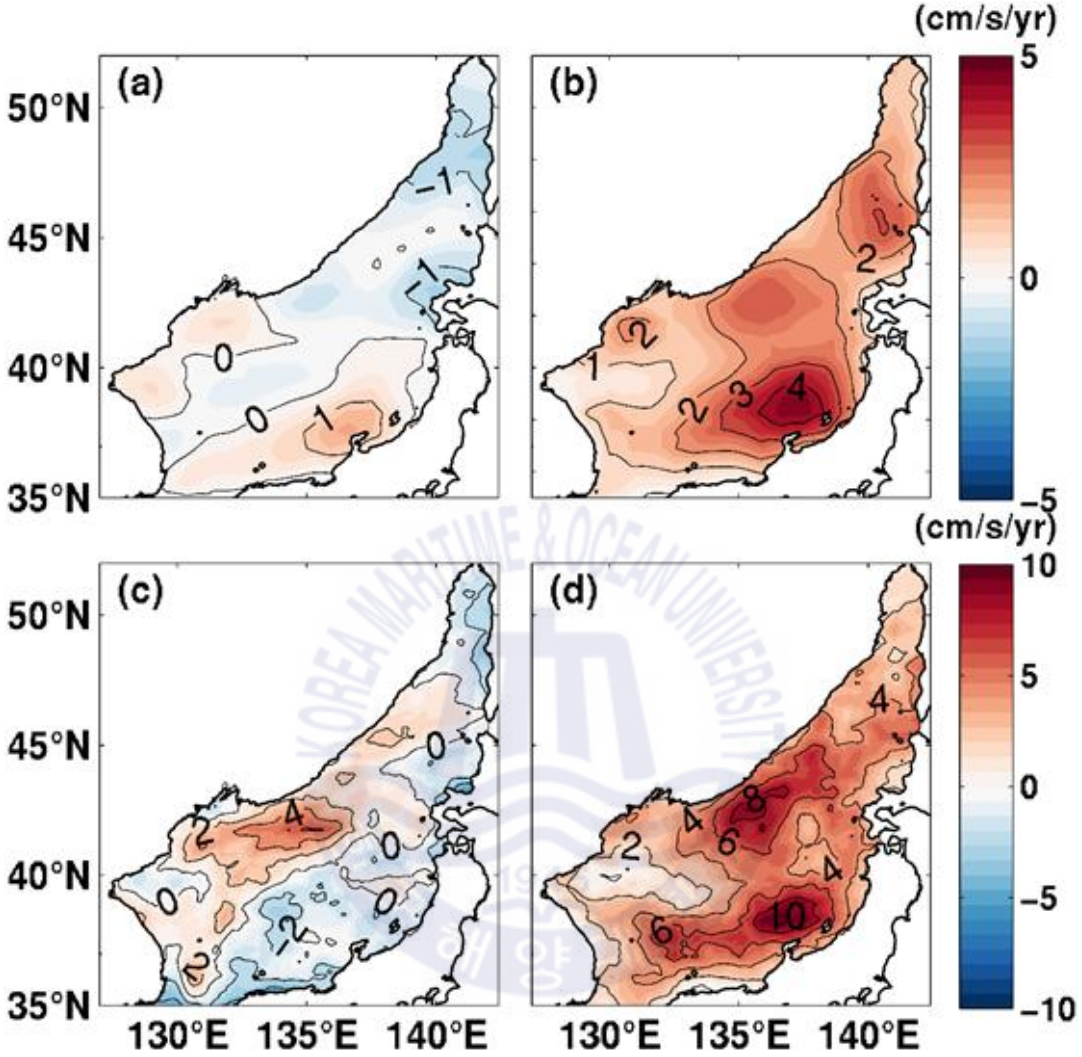

Fig. 8 Spatial distribution of trends of the monthly mean (upper) and 99th percentile (lower) wind speed in August (left panel) and December (right panel) in the East Sea over the period from 1979 to 2018.

Although spatial distribution of the trend of SWH similar to wind speed, it showed an increasing trend in the larger area than wind speed. In August, the monthly-mean SWH showed an increasing trend in the southern basin (1.0

mm/yr), and a decreasing trend in the northern basin (1.0 mm/yr) (fig 9a). The trends of the 99th percentile SWH and wind speed showed a similar characteristic: large amplitude of the trend and spatial pattern. From in the southwestern basin in the East Sea to northwestern basin along the coastline showed an increasing trend, while in the southeastern basin showed a maximum decreasing trend (13.6 mm/yr) (fig 9c). Trend of the SWH showed a decreasing trend (5.0 mm/yr) near the Ulsan, an increasing trend along the coast of Korea (5.0 mm/yr) and in the Korea Straits (22.4 mm/yr). In December, both monthly-mean and 99th percentile SWH also showed an increasing trend in most of the East Sea, particularly in the southeastern basin, the maximum of an increasing trend was 14.9 mm/yr, 54.0 mm/yr respectively (fig 9b, d). As the intensity of the Siberian High increased, the northwesterly winds became strong and the trend of SWH showed an increase sharply in the southeastern basin where has a long fetch length. Trend of the 99th percentile SWH in December increased significantly compared to that of August area mean (0.3 mm/yr, 14.4 mm/yr) and maximum value (22.4 mm/yr, 54.0 mm/yr). On the other hand, the coastline of Korea, both in August and in December showed an increasing trend (5.0 mm/yr).

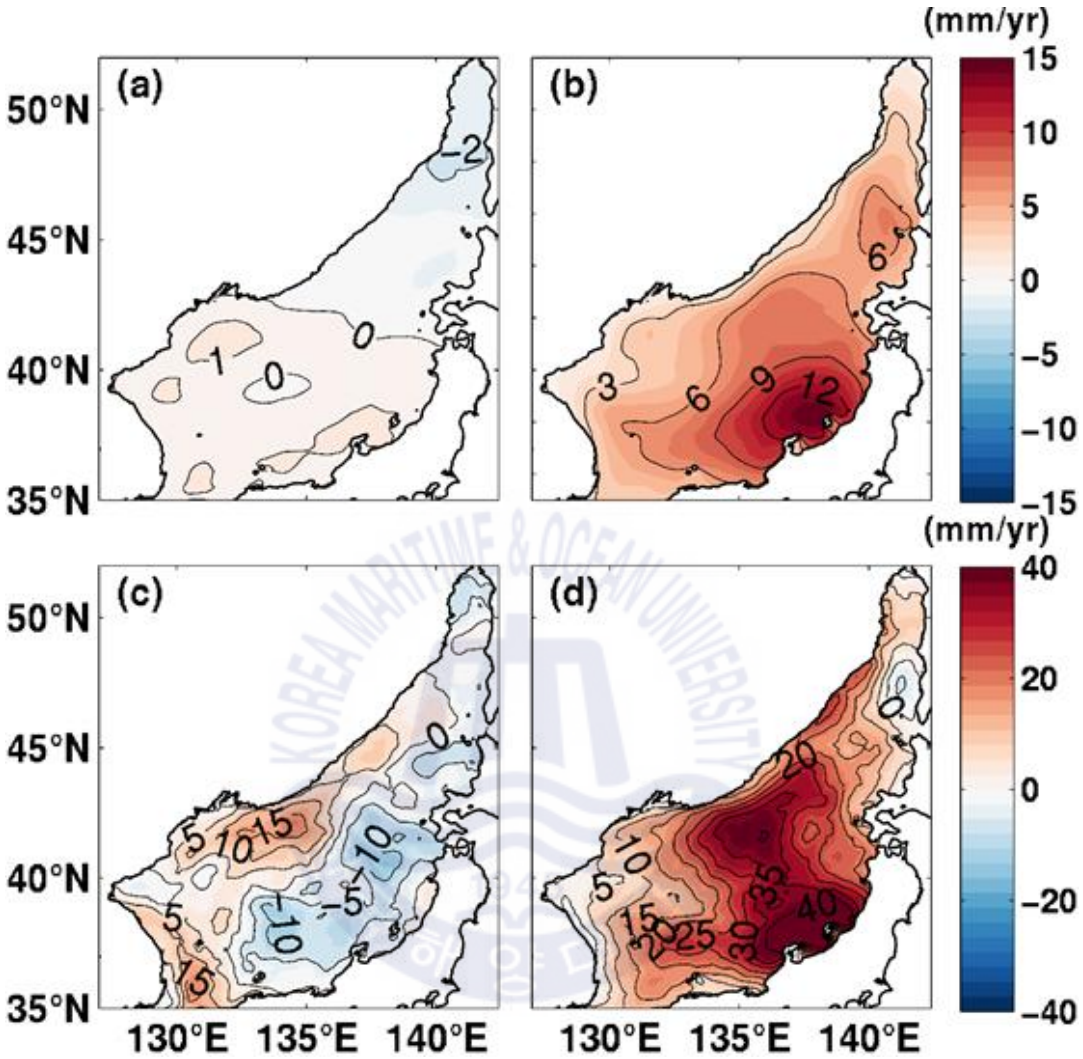

Fig. 9 Spatial distribution of trends of the monthly mean (upper) and 99th percentile (lower) significant wave height in August (left panel) and December (right panel) in the East Sea over the period from 1979 to 2018.

The trends of the monthly-mean and 99th percentile wind speed and SWH by areas showed similar monthly variation (fig 10). The trend of monthly-mean SWH showed an increasing intensely in February in the C area

and in March in the A and B areas, after then all of the areas appeared to decline increasing trend and incline increasing trend in December (fig 10c). The trend of the 99th percentile SWH significantly appeared monthly variation without in common (fig 10d). In area A, although the mean of the SWH and trend of monthly-mean SWH were lower than other areas (fig 5c, d), the trend of the 99th percentile SWH showed a sharply increasing in May, July, and October when other areas showed a slightly increasing or decreasing (fig 8d). The mean of SWH was high in the B area and wind speed was high in the C area, due to the difference in fetch length. The trends of the monthly-mean and 99th percentile wind speed (0.8 cm/s/yr, 2.6 cm/s/yr) and SWH (3.0 mm/yr, 11.0 mm/yr) in the B area appeared greater than wind speed (0.6 cm/s/yr, 1.3 cm/s/yr) and SWH (1.6 mm/yr, 3.7 mm/yr) in the C area. In area B, generally, the trend of SWH intensely increased than other areas, whereas the trend of monthly-mean SWH increased slightly and 99th percentile SWH decreased in May and August to October. In area C, the trend of SWH appeared the most frequently decreasing trend, especially, in October, the trend of 99th percentile SWH was -17.4 mm/yr as the largest decreasing trend. The maximum increasing trend of 99th percentile SWH was December except in the C area.

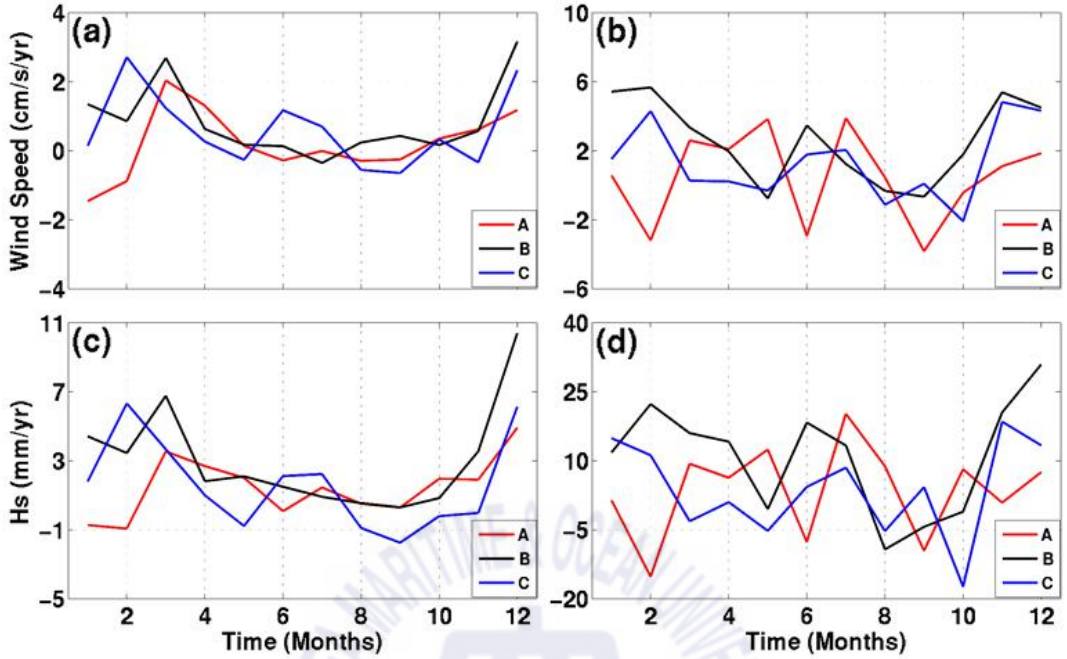

Fig. 10 Monthly variation of monthly mean (left panel) and 99th percentile (right panel) at three areas (A, B, & C) trend over 40 years (1979~2018): wind speed (upper) and significant wave height (lower).

3.2 99th percentile SWH, PWP, and PWD

3.2.1 Model validation

We validated the model result by the comparison with the buoy data at six locations (Ulleungdo northwest: UW, Ulleungdo northeast: UE, h105, h808, h809, h810) around the East Sea (fig 11). Among the six buoy data conducted by KHOA two data (UE, UW), which located in the East Sea, and of the observation data provided by NOWPHAS four data (h105, h808, h809, h810), whose depth is more than 50m were used (table 4). We used 2017 data that was the latest available wave data. To detect outlier of observation data using

Rosner test (Rosner, 1983), as a result, no outlier was found in the result ($p < 0.05$). To validate the model result, statistical analysis was performed of the SWH, PWP, PWD using bias, root mean square error: RMSE, correlation coefficient: ρ in each area. As a result, both SWH and PWP underestimated at all of six buoys, same as referred to 3.1.1. Both bias and RMSE of the SWH appeared higher value at NOWPHAS buoy than KHOA buoy due to the NOWPHAS buoy located in the southeastern basin where high SWH appeared. However, correlation coefficient was higher than 0.91. It means that the bias is high but the tendency is good, at NOWPHAS buoy.

Table 4 Information of the wave monitoring stations

Symbol	Station	Latitude(°N)	Longitude(°E)	Agency
UW	Ulleungdo northwest	38.0072	131.5525	KHOA
UE	Ulleungdo northeast	37.7427	130.6011	KHOA
h105	Wajima	37.4308	136.9022	NOWPHAS
h808	Sakata	38.9747	139.6006	NOWPHAS
h809	Akita	40.2106	139.6611	NOWPHAS
h810	Fukaura	40.7817	139.9375	NOWPHAS

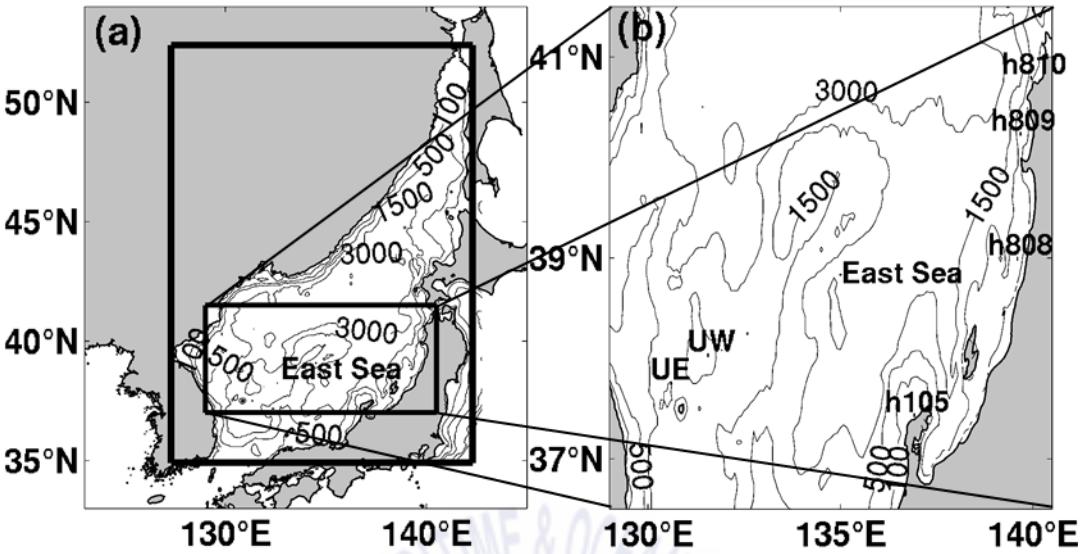

Fig. 11 (a) Model domain with bottom topography on a 1/25 ° × 1/25 ° grid. The black box represents the regions for detailed analysis. (b) Locations of the wave measurement stations (UW: Ulleungdo northwest, UE: Ulleungdo northeast, h105: Wajima, h808: Sakata, h809: Akita, h810: Fukaura) in the East Sea operated by KMA (Korea Meteorological Administration) and NOWPHAS (Nationwide Ocean Wave information network for Ports and HArborS).

Table 5 Statistics of modelled wave parameters (Hs, PWP, and PWD) at the six selected locations: mean, bias, root mean square error (RMSE), and correlation (ρ))

Location	Hs (m)				PWP (s)				PWD (N°)			
	mean	bias	RMSE	ρ	mean	bias	RMSE	ρ	mean	bias	RMSE	ρ
ULW	1.0604	-0.2408	0.4973	0.8883	4.6341	-0.9025	1.3807	0.8344	158.2990		0.5894	0.6758
ULE	1.1321	-0.2778	0.5453	0.8925	4.8138	-0.9596	1.4621	0.8212	153.6357		0.6094	0.6458
h105	0.7147	-0.4543	0.7106	0.9210	4.2210	-1.2283	2.0541	0.8150	154.6357		0.6435	0.2600
h808	0.9565	-0.4313	0.6426	0.9325	4.7700	-0.6704	1.4672	0.8366	252.7973		0.6004	0.4339
h809	1.0376	-0.5487	0.7718	0.9128	4.9358	-0.7746	1.4699	0.8158	249.5086		0.6809	0.4358
h810	1.0028	-0.5359	0.7409	0.9139	4.9128	-0.7880	1.5168	0.7508	246.0481		0.5507	0.5014

3.2.2 Long-term mean of wave properties

In this study, to investigate the spatiotemporal variation of the wave climate in the East Sea, analyzed wave properties (99^{th} percentile SWH, PWP, PWD) for the entire period and monthly. The 99^{th} percentile SWH showed high value (> 3.8 m) in the southeastern area, while low value (< 2 m) in the northwestern area (fig 12a). It is caused by high SWH occurred in the southeastern area where relatively fetch length is long. The monthly mean of the 99^{th} percentile SWH appeared that winter (December to February) and long-term mean showed a similar spatial distribution that increased from the northwestern to the southeastern basin (fig 12b). It means that spatial distribution of the long-term mean of 99^{th} percentile SWH affected by December. The entire area mean of the East Sea, the highest by 3.9 m in December, lowest by 2.1 m in June. The 99^{th} percentile SWH showed overall low (< 3 m) from May to August in which wind speed is weak, and high SWH in the center and southern basin, while showed overall high (> 3 m) in other months and high SWH in the southeastern basin. Although the 99^{th} percentile SWH varied depending on regions and seasons, in the southern basin is higher than the northern basin, and appeared low value from East Korea Bay to Tatar Strait throughout the year.

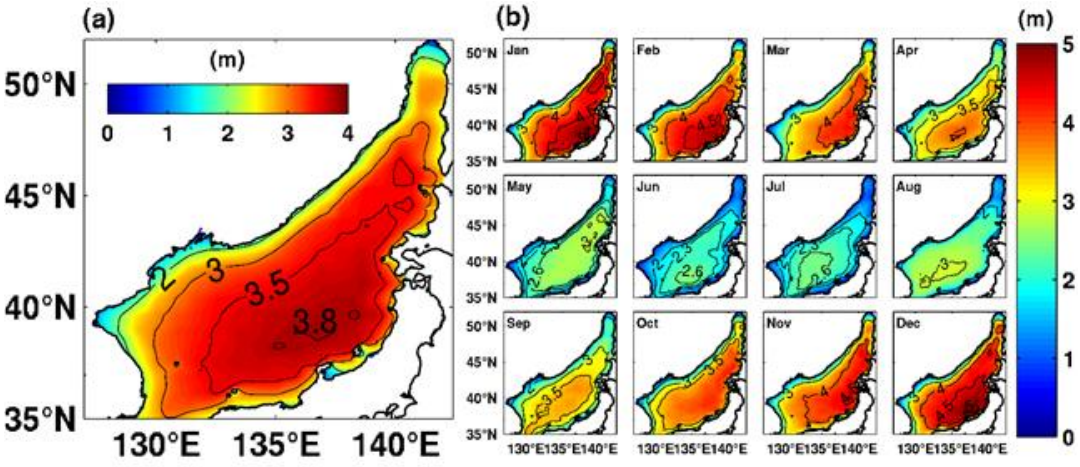

Fig. 12 Spatial distribution of (a) 40-year (1979~2018) mean, (b) monthly mean of 99th percentile significant wave height (m) in the East Sea.

The PWP appeared high value (> 4.9 s) in the southeastern area, while low value (< 4 s) in the northwestern area (fig 13a). It was similar spatial pattern with the 99th percentile SWH, because SWH and PWP have a positive correlation (fig 13b). While the 99th percentile SWH was observed high value above 47° N in the long-term and winter, the high value of PWP observed below 47° N overall. In summer PWP showed low value (< 4.1 s), other seasons showed high value (> 4 s). The entire area mean of the PWP was the longest in December at 5.3 s and the shortest in June at 3.8 s. From May to August in which wind speed is weak, the 99th percentile SWH showed the maximum value in the center and southern area, while PWP appeared the maximum value in the northern area.

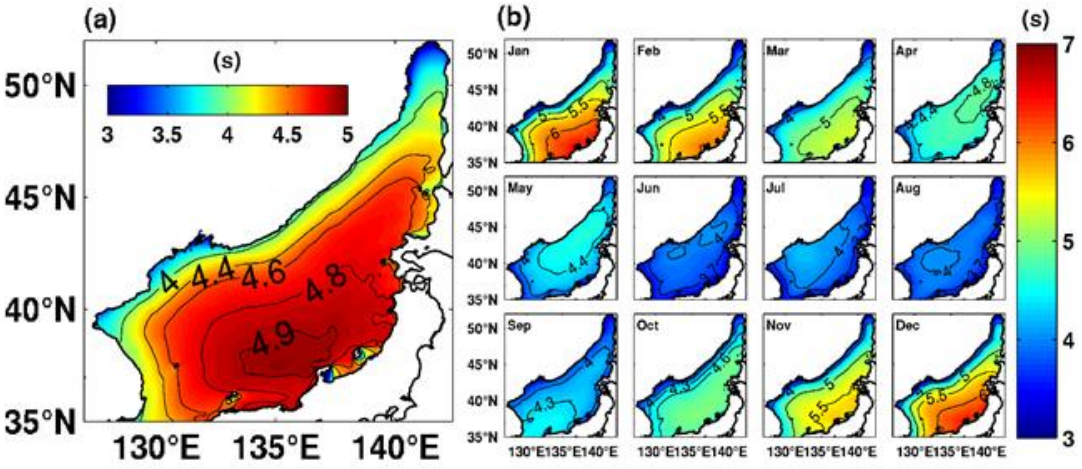

Fig. 13 Spatial distribution of (a) 40-year (1979~2018) mean, (b) monthly mean of peak wave period (s) in the East Sea.

The long-term mean of PWD was predominant from the northwesterly in the southeastern basin and altered an anti-clockwise toward coastal of Korea and Russia (fig 14a). As a result, the prevailing wave direction was northeasterly from Pohang to Uljin, and other regions the dominant wave was southeasterly. In winter, due to strong northwesterly wind, northwestern wave was dominant, exceptionally, there are predominant northeastern waves on the north coast of East Korea Bay and near Khabarovsk (fig 14b). In summer, due to southeasterly wind, the dominant waves are southeastern in the center and western basin. Owing to seasonal variability of wind, PWP, affected by wind speed, also showed apparent seasonal variability. Nevertheless, in the southeastern basin, the prevailing wave direction was northwest, and in the southwestern basin, from northeast to southeast waves are dominant throughout the year.

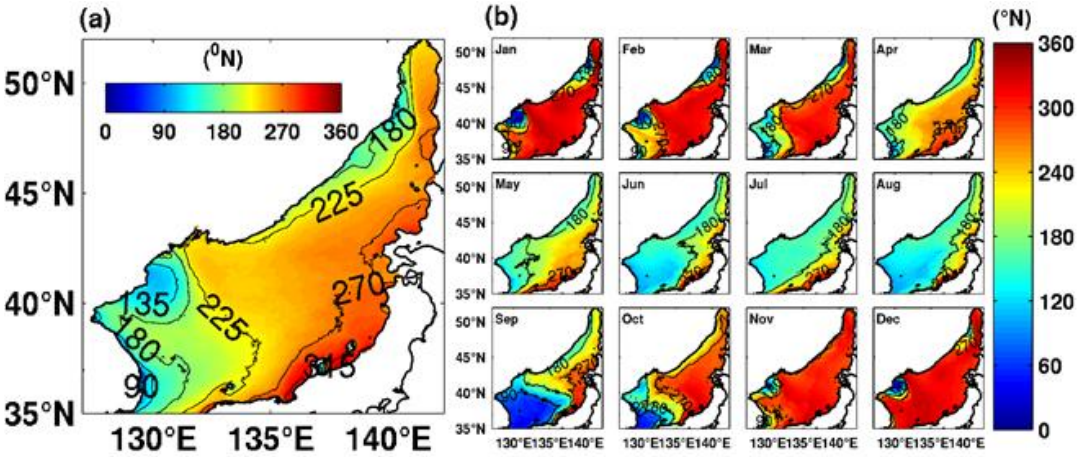

Fig. 14 Spatial distribution of (a) 40-year (1979~2018) mean, (b) monthly mean of peak wave direction (° N) in the East Sea.

3.2.3 Long-term trend of wave properties

Spatial distribution of the 99th percentile SWH and PWP was investigated by analyzing the long-term trend of wave climate. Except for the decreasing trend in the Korea East Bay (-2 cm/10 yr), the trend of the 99th percentile SWH appeared an increasing in most of the East Sea, especially, in the southeastern basin showed a maximum increasing (21 cm/10 yr) (fig 15a). The monthly increasing trend is the largest in December (54.0 cm/10 yr), followed by February (43.8 cm/10 yr) and January (36.9 cm/10 yr). A maximum decreasing trend was observed in October in the northeastern basin (-23.7 cm/10 yr), followed by February in the western basin (-22.9 cm/10 yr) and May in the eastern basin (-21.6 cm/10 yr). Spatial distribution of the trend of 99th percentile SWH substantially varied according to seasonal and regional. In February and June, an increased in the eastern area and in March, an increased in the southern area and a decreased in the northern area. In July, an increasing trend observed in most of the East Sea, and in August and

September increased in the northwestern area while decreased in the southeastern area, and in October appeared an increasing trend in the southwestern area and a decreasing trend in the eastern area. From November to January trends showed an increasing overall with a similar spatial pattern to the long-term trend and appeared a noticeable increasing trend in the southeastern area. Because due to the Siberian high became intensity, the northwesterly wind strengthened. Generally, while the trend of the 99th percentile SWH showed increasing in the southeastern basin, in August and September showed a decreasing in the southeastern basin. Except in February, June, and September, the 99th percentile SWH showed an increasing trend on the coast of Korea.

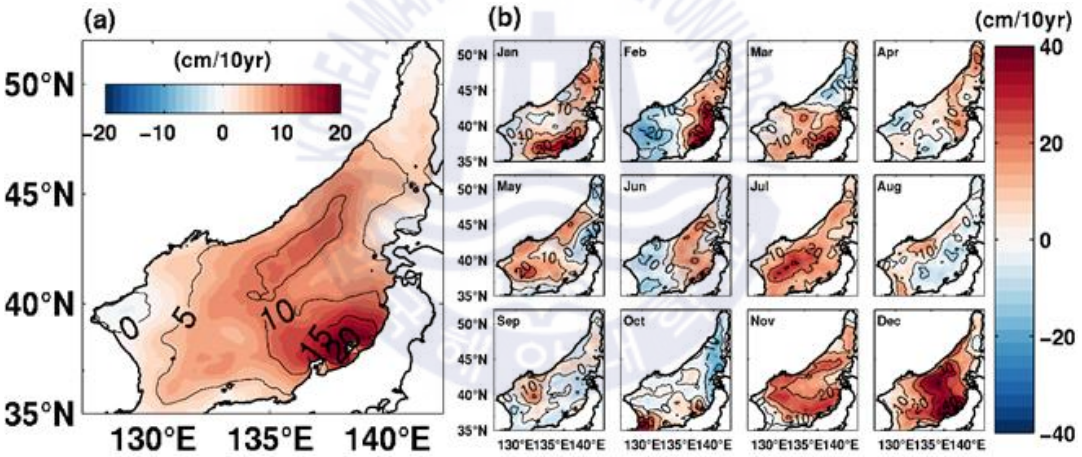

Fig. 15 Spatial distribution of (a) linear trends, (b) monthly trends of 99th percentile significant wave height in the East Sea over the period from 1979 to 2018.

The long-term trend of PWP increased overall, the exception of near Khabarovsk (fig 16a). The maximum increasing trend was located in the southeastern area (0.08 s/10 yr), and a high increasing trend showed in the

southwestern area (0.06 s/10 yr) and near Soya Straits (0.04 s/10 yr). Although spatial distribution of the long-term and monthly mean of PWP showed similar to the 99th percentile SWH, the linear trend showed differently. Contrary to the trend of the 99th percentile SWH that significantly varied depending on seasons and locations, the PWP showed an increasing trend over the longer period and wider area (fig 16b). The monthly trend of PWP increased overall, the exception of the western coast in March, northwestern coast in April, eastern coast in May, and northern area from August to October. Except in March, the PWP appeared an increasing trend on the coast of Korea, especially, in January and October, there was a remarkable increasing trend (0.14 s/10 yr) in the southern area. The increasing trend of the 99th percentile SWH was more decreasing toward the coast, that of the PWP was more increasing toward the coast.

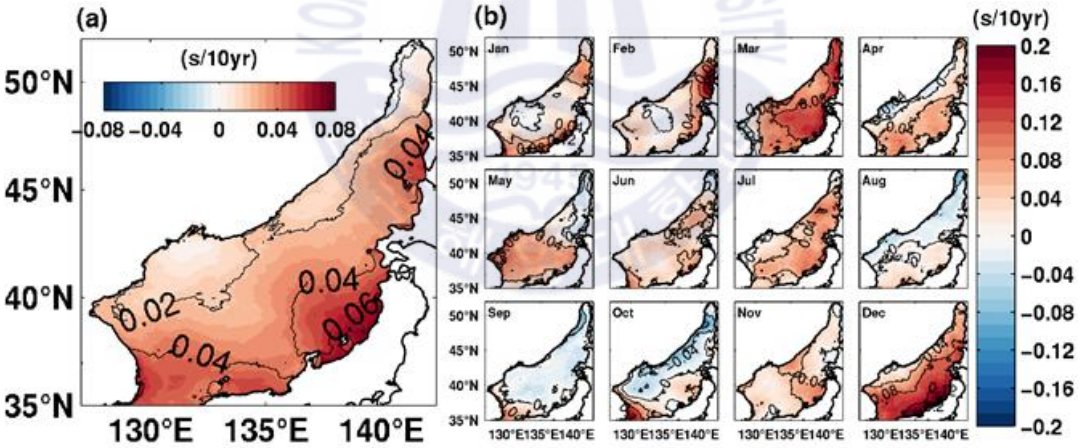

Fig. 16 Spatial distribution of (a) linear trends, (b) monthly trends of peak wave period in the East Sea over the period from 1979 to 2018.

4. Discussion and conclusion

Swelling waves are large-height and long-period waves that suddenly invaded the coastline before and after the storm occurred from October to April. Jeong et al. (2007) defined the swelling waves: extratropical cyclone migrated the East Sea, the central pressure drastically decreased after that, a strong pressure trough was created near extratropical cyclone, wind speed became stronger, as a result, it is wave invading the east coast of Korea from October to April. To express this quantitatively, Oh et al. (2010) defined that the waves of more than 3 m in height and more than 9 s in period invaded continuously the coast for more than several hours in winter. Swelling waves were more frequent than summer high waves generated by typhoons, and it is difficult to predict because it suddenly invaded regardless of coastal weather and sea conditions. Therefore, most previous research studied swelling waves in winter (Oh et al., 2010; Chun et al., 2014). Wind speed in winter is faster than that of summer, so SWH is high in winter. On the other hand, when typhoons passed, wind speed sharply strong, wind speed in this period was faster than that of winter. High SWH affected by typhoons was higher than swelling waves were generated in winter. Due to climate changes, the number of typhoons decreased and intensity increased, it is expected that high SWH generated by typhoons more affect the coast of Korea. So, we considered that more future research needs to study high SWH produced by typhoons.

Both monthly-mean and 99^{th} percentile SWH appeared increasing trend in the East Sea, but the 99^{th} percentile SWH was more intensified than the

monthly-mean SWH. In August, the monthly-mean and 99th percentile SWH area means were 0.1 mm/yr, 0.3 mm/yr respectively, maximum values were 1.7 mm/yr, 22.4 mm/yr respectively. In December, area means were 5.9 mm/yr, 14.4 mm/yr respectively, maximum values were 14.9 mm/yr, 54.0 mm/yr respectively. The amplitudes of the 99th percentile SWH were 2 to 3 times as large as the monthly-mean SWH. High SWH trends are more positive than mean SWH not only in the East Sea but also in other regions with the high latitudes (greater than 35° N) (Ruggiero et al., 2010b; Young, 2011).

In August, the 99th percentile wind speed and SWH showed an increasing trend from the southwestern to the northwestern area. It seemed that the intensity and the number of typhoons passed the East Sea increased. In general, a high wave was generated when blowing strong wind speed, and the extreme condition of wind speed and SWH had a strong correlation (Young, 2011), so, the 99th percentile wind speed and SWH showed a similar pattern.

In December, the trends of the 99th percentile wind speed and SWH appeared increasing in most of the area, particularly, the largest increase showed the southeastern area. Because the intensity of the Siberian High increased, the northwesterly wind became strong and the trend of SWH increased. The trend of the 99th percentile SWH increased in the wider area relatively. In winter due to the strong northwesterly winds blew continuously, increasing the fetch length from the northwestern to the southeastern basin, thus, it seemed that although the increasing trend of wind speed was weak, that of SWH was strong. As a result of analyzing the mean and trends of the wind speed and SWH by areas, that of SWH were influenced by wind speed dominantly. Therefore, we suggest that if we improve the spatiotemporal resolution of wind data, it is possible to accurately analyze the regional difference in SWH in the East Sea.

The monthly wind variation significantly due to the monsoon, therefore the

wave properties, affected by wind, also appeared large spatiotemporal variation. Whereas the trends of the 99th percentile SWH and PWP increased on the coast of Korea, except in February, June, September, and March respectively. The long-term mean of PWD was predominant northeasterly except for summer which dominant southeast wind. Dominant PWD was northeast and the increasing trends of the monthly-mean and 99th percentile SWH and PWP, so we guess that influences on the coastal environment of the east coast will be significant. In addition, as the trends of 99th percentile SWH and PWP increased in most of the region, it is expected that the swelling waves, large-height and long-period waves, invade in winter that it will be a greater influence the east coast.

In this study, to investigate a long-term mean and linear trend of wave properties in the East Sea by using the SWAN wave model forced with ECMWF reanalysis wind data during 40 years (1979~2018) wave hindcast experiment. The limitation of this study was that it used only wind field and bathymetry data without boundary condition, and model result underestimated the observation buoy data. Future studies will include other factors, such as current, SST, and reduce bias with observation value.

Climate change transmuted the wave climate including wave direction which could lead to sediment supply variability and coastal erosion (Van Lancker et al., 2004; Slott et al., 2006; Ruggiero et al., 2010a; Park et al., 2014; Ranasinghe, 2016; Anderson et al., 2018). If we will study PWD which is wave direction with high spectrum energy, it is though to be able to mitigate coastal erosion and change, by the wave. However, different from wave height and period which have less variation with a constant value, wave direction has large variation so it needs to study how to analyze the trend. Future wave climate changes due to climate change, so projecting variation of the wave characteristics using the future wind data and based on the results,

it will be helpful in establishing a strategy and coastal erosion reduction. Therefore, it is necessary to study the projection of future climate change.

감사의 글

이 글을 마지막으로 3년간의 석사과정이 끝이 났습니다. 학부를 졸업하고 공부를 더 해보고 싶다는 생각으로 대학원에 진학하였습니다. 3년이라는 짧지 않은 기간 동안 여러 일들을 겪으면서 많은 것을 배웠습니다. 연구에 대해 아무것도 모르던 저를 여기까지 올 수 있도록 지도해주신 장찬주 박사님 감사합니다. 파랑 모형에 대해 하나하나 알려주시고 많은 도움을 주신 도기덕 교수님 감사합니다. 연구와 관련된 용어와 기본 개념 등의 중요성을 알려주시고 논문을 심사해 주신 유제선 박사님 감사합니다. 논문 그림과 미래에 대해 도움이 되는 말씀을 많이 해주신 김용선 박사님 감사합니다. 과 후배라고 많이 챙겨주시고 여러 도움 주신 성봉 형 감사합니다. 매번 말했지만 정말 형 덕분에 늦게까지 하며 논리적으로 많은 도움을 받았습니다. 매트랩 코드와 컴퓨터로 고생하고 있을 때마다 도와준 희석 형 감사합니다. 연구소에 몇 없는 또래가 같은 실험실 사람이었던 민경 누나, 원근 힘들 때 많은 의지가 되어 좋았습니다. 이 글에 이름을 담지 못한 많은 분들께 진심으로 감사의 말씀을 드립니다. 덕분에 힘든 대학원 생활에 즐거움을 느끼고 힘이 되었습니다.

마지막으로 항상 뒤에서 응원해 주시고 기다려주신 부모님께 감사하다는 말씀 드립니다.

Reference

최진렬, 이시경, 2010. 너울성 파도에 대한 재난관리 과정분석: 강릉 안목항 사고와 보령 죽도 사고를 중심으로. *한국공공관리학보*, 24(2), pp.71-98.

Akpinar, A., van Vledder, G.P., Komurcu, M.I., and Ozger, M., 2012. Evaluation of the numerical wave model (SWAN) for wave simulation in the Black Sea. *Continental Shelf Research*, 50, pp.80-99.

Allan, J., and Komar, P., 2000. Are ocean wave heights increasing in the eastern North Pacific?. *Eos, Transactions American Geophysical Union*, 81(47), pp.561-567.

Anderson, D., Ruggiero, P., Antolinez, J.A., Mendez, F.J., and Allan, J., 2018. A climate index optimized for longshore sediment transport reveals interannual and multidecadal littoral cell rotations. *Journal of Geophysical Research: Earth Surface*, 123(8), pp.1958-1981.

Becker, J.J., Sandwell, D.T., Smith, W.H.F., Braud, J., Binder, B., Depner, J., Fabre, D., Factor, J., Ingalls, S., Kim, S.H., Ladner, R., Marks, K., Nelson, S., Pharaoh, A., Trimmer, R., Von Rosenberg, J., Wallace, G., and Weatherall, P., 2009. Global bathymetry and elevation data at 30 arc seconds resolution: SRTM30_PLUS. *Marine Geodesy*, 32(4), pp.355-371.

Booij, N., Ris, R.C., and Holthuijsen, L.H., 1999. A third-generation wave model for coastal regions: 1. Model description and validation. *Journal of Geophysical Research*, 104(C4), pp.7649-7666.

Caires, S., Kim, J., and Groeneweg, J., 2018. Korean East Coast wave predictions by means of ensemble Kalman filter data assimilation. *Ocean Dynamics*, 68(11), pp.1571-1592.

Cardone, V.J., Jensen, R.E., Resio, D.T., Swail, V.R., and Cox, A.T., 1996. Evaluation of contemporary ocean wave models in rare extreme events: the "Halloween storm" of October 1991 and the "Storm of the century" or March 1993. *Journal of Atmospheric and Oceanic Technology*, 13(1), pp.198-230.

Castelle, B., Dodet, G., Masseling, G., and Scott, T., 2018. Increased winter-mean wave height, variability, and periodicity in the Northeast Atlantic over 1949-2017. *Geophysical Research Letters*, 45, pp.3586-3596.

Cavaleri, L., and Malanotte-Rizzoli, P., 1981. Wind wave prediction in shallow water: Theory and applications, J*ournal of Geophysical Research: Oceans*, 86(C11), pp.10961-10973.

Cavaleri, L., 2009. Wave modeling-Missing the peaks. *Journal of Physical Oceanography*, 39(11), pp.2757-2778.

Charles, E., Idier, D., Thiebot, J., Le Cozannet, G., Pedreros, R., Ardhuin, F., and Planton, S., 2012. Present wave climate in the Bay of Biscay: spatiotemporal variability and trends from 1958 to 2001. *Journal of Climate*, 25(6), pp.2020-2039.

Chen, G., Chapron, B., Ezraty, R., and Vandemark, D., 2002. A global view of swell and wind sea climate in the ocean by satellite altimeter and scatterometer. *Journal of Atmospheric and Oceanic Technology*, 19(11), pp.1849-1859.

Chun, J.H., Ahn, K.M., Suh, K.D., and Yoon, J.T., 2011. Application of dynamically coupled POM-WAM to undertow simulation. *Journal of Korean Society of Coastal and Ocean Engineers*, 23(2), pp.182-191.

Chun, H., Kang, T.S., Ahn, K., Jeong, W.M., Kim, T.R., and Lee, D.H., 2014. A study on the statistical characteristics and numerical hindcasts of storm waves in East Sea. J*ournal of Korean Society of Coastal and Ocean Engineers*, 26(2), pp.81-95.

Cox, A.T., and Swail, V.R., 2001. A global wave hindcast over the period

1958-1997: Validation and climate assessment. *Journal of Geophysical Research: Oceans*, 106(C2), pp.2313-2329.

Do, K., and Kim, J., 2018. A study of the Predictability of Eastern winter storm waves using operational wind forecasts of KMA. *Journal of Korean Society of Coastal and Ocean Engineers*, 30(5), pp.223-233.

Dodet, G., Bertin, X., and Taborda, R., 2010. Wave climate variability in the North-East Atlantic Ocean over the last six decades. *Ocean modelling*, 31(3-4), pp.120-131.

Duan, W., He, B., Takara, K., Luo, P., Hum M., Alias, N.E., Ishihara, M., and Wang, Y., 2014. Climate change impacts on wave characteristics along the coast of Japan from 1986 to 2012. J*ournal of Coastal Research*, 68(sp1), pp.97-104.

Dupis, H., Michel, D., and Sottolichio, A., 2006. Wave climate evolution in the Bay of Biscay over two decades. *Journal of Marine Systems*, 63(3-4), pp.105-114.

Ebuchi, N., Kawamura, H., and Toba, Y., 1992. Growth of wind waves with fetch observed by the Geosat altimeter in the Japan Sea under winter monsoon. J*ournal of Geophysical Research: Oceans*, 97(C1), pp.809-819.

Ebuchi, N., 1999. Growth of wind waves with fetch in the Sea of Japan under winter monsoon investigated using data from satellite altimeters and scatterometer. *Journal of Oceanography*, 55(5), pp.575-584.

Emanuel, K., 2005. Increasing destructiveness of tropical cyclones over the past 30 years. *Nature*, 436(7051), pp.686-688.

Gamo, T., and Horibe, Y., 1983. Abyssal circulation in the Japan Sea. *Journal of the Oceanographical Society of Japan*, 39(5), pp.220-230.

Go, J.S., An, I.J., and Eom, H.M., 2006. Damage by swell in eastern coasts of Korean Peninsula. *Korean Society of Hazard Mitigation*, 6, pp.57-64.

Goda, Y. (2003), Revisiting Wilson's formulas for simplified wind-wave prediction. *Journal of waterway, port, coastal, and ocean engineering*, 129(2),

pp.93-95.

Harley, M.D., Tuner, I.L., Short, A.D., Ranasinghe, R., 2010. Interannual variability and controls of the Sydney wave climate. *International Journal of Climatology*, 30(9), pp.1322-1355.

Hemer, M.A., Fan, Y., Mori, N., Semedo, A., Wang, X.L., 2013. Projected changes in wave climate from a multi-model ensemble. *Nature Climate Change*, 3(5), pp.471.

Heo, K.Y., Ha, T., Choi, J.Y., Park, K.S., Kwon, J.I., and Jun, K., 2017. Evaluation of wind and wave simulations using different global reanalyses. *Journal of Coastal Research*, 79(sp1), pp.99-103.

Janssen, P.A., 1989. Wave-induced stress and the drag of air flow over sea waves. *Journal of Physical Oceanography*, 19(6), pp.745-754.

Janssen, P.A., 1991. Quasi-linear theory of wind-wave generation applied to wave forecasting. *Journal of Physical Oceanography*, Vol 21(11), pp.1631-1642.

Jeong, W.M., Oh, S.H., Lee, D.Y., 2007. Abnormally high waves on the east coast. *Journal of Korean Society of Coastal and Ocean Engineers*, 19(4), pp.295-302.

Jeong, W.M., and Oh, S.H., 2009. Abnormally high swells occurred on the east coast in recent several years. *2009 Conference of the Korean Association of Ocean Science and Technology Societies*, pp.2119-2122.

Jeong, W.M., Ryu, K.H., Cho, H., 2015. Long-term wave monitoring and analysis off the coast of Sokcho. *Journal of Korean Society of Coastal and Ocean Engineers*, 27(4), pp.274-279.

Jeong, W.M., Oh, S.H., and Eum, H,S., 2016. Analysis of wave climate around Korea based on long-term hindcast and coastal observation data. *Journal of Coastal Research*, Vol 75(sp1), pp.735-740.

Kang, T.S., Park, J.J., and Eum, H.S., 2016. Wave tendency analysis on the coastal waters of Korea using wave hind-casting modelling. *Journal of the*

Korean Society of Marine Environment & Safety, 22(7), pp.869-875.

Kazeminezhad, M.H., and Siadatmousavi, S.M., 2017. Performance evaluation of WAVEWATCH III model in the Persian Gulf using different wind resources. *Ocean Dynamics*, 67(7), pp.839-855.

Kim, G., Jeong, W.M., Lee, K.S., Jun, K., and Lee, M.E., 2011. Offshore and nearshore wave energy assessment around the Korean Peninsula, *Energy*, 36(3), pp.1460-1469.

Kim, K.O., Lee, H.S., Min, B.I., and Choi, B.H., 2011. Hindcating of high swell waves off the eastern Korean coast on 24 February 2008 using structured and unstructured wave models. *Journal of Coastal Research*, pp.1073-1077.

Kim, Y.S., Jang, C.J., and Yeh, S.W., 2018. Recent surface cooling in the Yellow and East China Seas and the associated North Pacific climate regime shift. *Continental Shelf Research*, 156, pp.43-54.

Komen, G,J., Hasselmann, K., and Hasselmann, K., 1984. On the existence of a fully developed wind-sea spectrum, *Journal of Physical Oceanography*, 14(8), pp.1271-1285.

Mei, W., Xie, S.P., Primeau, F. McWilliams, J.C., and Pasquero, C., 2015. Northwestern Pacific typhoon intensity controlled by changes in ocean temperatures. *Science Advances*, 1(4), pp.e1500014.

Oh, S.H., Jeong, W.M., Lee, D.Y., and Kim, S.I., 2010. Analysis of the reason for occurrence of large-height swell-like waves in the east coast of Korea. *Journal of Korean Society of Coastal and Ocean Engineers*, 22(2), pp.101-111.

Pallares, E., Sanchez-Arcilla, A., and Espino, M., 2014. Wave energy balance in wave models (SWAN) for semi-enclosed domains-application to the Catalan coast. *Continental Shelf Research*, 87, pp.41-53.

Park, J.S., Kang, K., Kang, H.S., and Kim, Y.H., 2013. Projection of the future wave climate changes over the Western North Pacific. *Journal of Korean Society of Coastal and Ocean Engineers*, 25(5), pp.267-275.

Park, J., Khim, K.B., Lee, H.J., and Lee, S.R., 2014. Recent morphological

changes off the shoreface of Jinwoodo and Sinjado in the Nakdong river estuary: 2007-2012. *Ocean and Polar Research*, 36(2), pp.87-101.

Pierson, W.J., and Moskowitz, L., 1964. A proposed spectral from for fully developed wind seas based on the similarity theory of SA Kitaigorodskii. *Journal of Geophysical Research*, 69(24), pp.5181-5190.

Raamet, A., Soomere, T., and Zaitseva-Parnaste, I., 2010. Variations in extreme wave hiehgts and wave directions in the north-eastern Baltic Sea. *Proceedings of the Estonian ACademy of Sciences*, 59(2).

Ranasinghe, R., 2016. Assessing climate change impacts on open sandy coasts: A review. *Earth-Science Reviews*, 160, pp.320-332.

Ris, R.C., Holthuijsen, L.H., and Booij, N., 1999. A third-generation wave model for coastal regions: 2. Verification. *Journal of Geophysical Research: Oceans*, 104(C4), pp.7667-7681.

Rosner, B., 1983. Percentage points for a generalized ESD many-outlier procedure. *Technometrics*, 25(2), pp.165-172.

Ruggiero, P., Buijsman, M., Kaminsky, G.M., and Gelfenbaum, G., 2010. Modeling the effects of wave climate and sediment supply variabiliry on large-scale shoreline change. *Marine Geology*, 273(1-4), pp.127-140.

Ruggiero, P., Komar, P.D., and Allan, J.C., 2010. Increasing wave heights and extreme value projections: The wave climate of the US Pacific Northwest. *Coastal Engineering*, 57(5), pp.539-552.

Sasaki, W., Iwasaki, I., Matsuura, T., and Iizuka, S., 2005. Recent increase in summertime extreme wave heights in the western North Pacific. *Geophysical Research Letters*, 32(15), L15607.

Seol, D.I., 2010. Global warming and trends of typhoon variation. *Journal of Navigation and Port Research*, 34(6), pp.453-458.

Shimura, T., Mori, N., and Hemer, M.A., 2016. Variability and future decreases in winter wave heights in the Western North Pacific. *Geophysical Research Letters*, 43(6), pp.2716-2722.

Simmons, A., Ullala, S., Dee, D., and Kobayashi, S., 2006. ERA-Interim: New ECMWF reanalysis products from 1989 onwards. *ECMWF Newsletter*, 110, pp.25-36.

Slott, J.M., Murray, A.B., Ashton, A.D., and Crowley, T.J., 2006. Coastline responses to changing storm patterns, *Geophysical Research Letters*, 33(18).

Suh, K,D., Kwon, H,D., and Lee, D.Y., 2010. Some statistical characteristics of large deepwater waves around the Korean Peninsula. *Coastal Engineering*, 57(4), pp.375-384.

Suh, K.D., Kim, M.J., and Chun, J.H., 2011. Estimation of deepwater design wave height on southern coast of Korean peninsula by empirical simulation etchnique. Journal of Korean Society of Coastal and Ocean Engineers, 23(4), pp.265-275.

Sun, L., Perlwitz, J., and Hoerling, M., 2016. What caused the recent "Warm Arctic, Cold Continents" trend pattern in winter temperatures?. *Geophysical Research Letters*, 43(1), pp.5345-5352.

Tolman, H.L., 1992. Effects of numerics on the physics in a third-generation wind-wave model. *Journal of Physical Oceanography*, 22(10), pp.1095-1111.

Van Lancker., Swail, V.R., Hearn, S., Hoekstra, P., Levoy, F., Miles, J., Moerkerke, G., Monfort, O., and Whitehouse, R., 2004. Coastal and nearshore morphology, bedforms and sediment transport pathways at Tegnmouth (UK). *Continental Shelf Research*, 24(11), pp.1171-1202.

U.S. Army Coastal Engineering Research Center., 1977. Shore protection manual, 3rd ed. *U.S. Government Printing Office, Washington, DC.*

Wang, X.L., and Swail, V.R., 2002. Trends of Atlantic wave extremes as simulated in a 40-yr wave hindcast using Kinematically reanalyzed wind fields. *Journal of Climate*, 15(9), pp.1010-1035.

Webster, P.J., Holland, G.J., Curry, J.A., and Chang, H.R., 2005. Changes in tropical cyclone number, duration, and intensity in a warming environment. *Science*, 309(5742), pp.1844-1846.

Weisse, R., and Gunther, H., 2007. Wave climate and long-term changes for the Southern North Sea obtained from a high-resolution hindcast 1958-2002. *Ocean Dynamics*, 57(3), pp.161-172.

Woo, H.J., and Park. K.A., 2017. long-term trend of satellite-observed significant wave height and impact on ecosystem in the East/Japan Sea. *Deep Sea Research Part II*, 143, pp.1-14.

Wu, M.C., Yeung, K.H., and Chang, W.L., 2006. Trends in western North Pacific tropical cyclone intensity. *Eos, Transactions American Geophysical Union*, 87(48), pp.537-538.

Yamaguchi, M., and Hatada, Y., 2002. 51-year wave hindcast and analysis of wave height climate trend of the Northwestern Pacific ocean. Proc. *7th int. Workshop on Wave Hindcasting and Forecasting*, pp.60-69.

Young, I.R., 1994. Global ocean wave statistics obtained from satellite observations. *Applied Ocean Research*, 16(4), pp.235-248.

Young, I.R., Zieger, S., and Babanin, A.V., 2011. Global trends in wind speed and wave height. *Science*, 332(6028), pp.451-455.

Zhao, S., Feng, T., Tie, X., Long, X., Li, G., Cao, J., Zhou, W., and An, Z., 2018. Impact of climate change on Siberian High and wintertime air pollution in China in past two decades. *Earth's Future*, 6(2), pp.118-133.

Zheng, C., Zhou, L., Huang, C., Shi, Y., Li, J., and Li, J., 2013. The long-term trend of the sea surface wind speed and the wave height (wind wave, swell, mixed wave) in global ocean during the last 44 a. *Acta oceanologica sinica*, 32(10), pp.1-4.

Zheng, C.W., and Li, C.Y., 2015. Variation of the wave energy and significant wave height in the China Sea and adjacent waters. *Renewable and Sustainable Energy Reviews*, 43, pp.381-387.